

# Effect of Inorganic Salts on N-Containing Organic Compounds Formed by Heterogeneous Reaction of NO<sub>2</sub> with Oleic Acid

Huifan Deng, Jiangping Liu, Yiqun Wang, Wei Song, Xinming Wang, Xue Li,\* Davide Vione, and Sasho Gligorovski\*



Cite This: *Environ. Sci. Technol.* 2021, 55, 7831–7840



Read Online

ACCESS |



Metrics & More

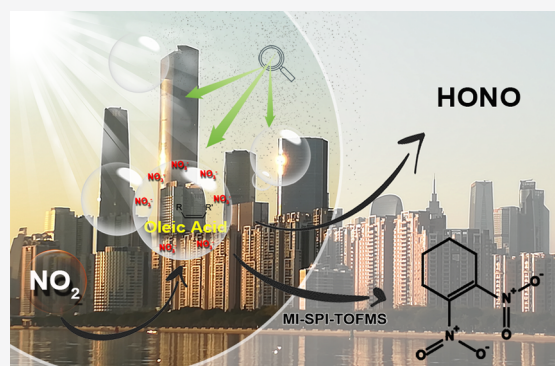


Article Recommendations



Supporting Information

**ABSTRACT:** Fatty acids are ubiquitous constituents of grime on urban and indoor surfaces and they represent important surfactants on organic aerosol particles in the atmosphere. Here, we assess the heterogeneous processing of NO<sub>2</sub> on films consisting of pure oleic acid (OA) or a mixture of OA and representative salts for urban grime and aerosol particles, namely Na<sub>2</sub>SO<sub>4</sub> and NaNO<sub>3</sub>. The uptake coefficients of NO<sub>2</sub> on OA under light irradiation (300 nm < λ < 400 nm) decreased with increasing relative humidity (RH), from (1.4 ± 0.1) × 10<sup>-6</sup> at 0% RH to (7.1 ± 1.6) × 10<sup>-7</sup> at 90% RH. The uptake process of NO<sub>2</sub> on OA gives HONO as a reaction product, and the highest HONO production was observed upon the heterogeneous reaction of NO<sub>2</sub> with OA in the presence of nitrate (NO<sub>3</sub><sup>-</sup>) ions. The formation of gaseous nitroaromatic compounds was also enhanced in the presence of NO<sub>3</sub><sup>-</sup> ions upon light-induced heterogeneous processing of NO<sub>2</sub> with OA, as revealed by membrane inlet single-photon ionization time-of-flight mass spectrometry (MI-SPI-TOFMS). These results suggest that inorganic salts can affect the heterogeneous conversion of gaseous NO<sub>2</sub> on fatty acids and enhance the formation of HONO and other N-containing organic compounds in the atmosphere.



**KEYWORDS:** oleic acid, heterogeneous reactions, nitrogen oxides, nitrous acid, nitroaromatic compounds, urban air pollution, indoor air

## INTRODUCTION

Atmospheric aerosol particles are loaded with organic and inorganic compounds.<sup>1</sup> Organic compounds can affect the optical properties and hygroscopic growth of aerosol particles, and they can influence the heterogeneous reactions between oxidant species and inorganic constituents.<sup>2</sup> Among the organic compounds, fatty acids are emitted in the air by coal burning<sup>3</sup> and cooking.<sup>4–6</sup> Fatty acids represent one important portion of the organic compounds in aerosol and because of amphiphilic properties and poor solubility in the aqueous phase, they act as surfactants and have the ability to create a coating over the aerosol particle core.<sup>7</sup> The surface of aerosols that mainly contain sulfate (SO<sub>4</sub><sup>2-</sup>) and nitrate (NO<sub>3</sub><sup>-</sup>) can, for instance, be enriched with unsaturated fatty acids.<sup>8</sup> Oleic acid (OA, C<sub>18</sub>H<sub>34</sub>O<sub>2</sub>) or 9-octadecenoic acid is an unsaturated fatty acid that is routinely detected in aerosol particles and can be used as a marker compound for cooking.<sup>9,10</sup> Recently, real-time measurements in indoor environments detected over 600 compounds among primary emitted cooking compounds and secondary products formed by reactions with hydroxyl radicals (OH).<sup>11</sup> Among all the detected compounds, 183 features were identified as unsaturated or saturated fatty acids, and OA was the most abundant unsaturated fatty acid.<sup>11</sup> The reaction of ozone with OA as a proxy for unsaturated fatty acids has been comprehensively evaluated in the past to better

understand the oxidation processes affecting aerosol particles.<sup>12–20</sup> Studies have also been carried out on the oxidative processing of OA by other relevant atmospheric oxidants (radicals) such as hydroxyl (OH),<sup>21</sup> nitrate (NO<sub>3</sub>),<sup>14</sup> and chlorine (Cl).<sup>22</sup>

The organic compounds adsorbed on urban grime can be oxidized by atmospheric oxidants and affect urban air quality.<sup>23,24</sup> In addition to the fatty acids and polycyclic aromatic hydrocarbons (PAHs), urban grime contains salts such as nitrate and sulfate that are major species in grime and are very stable within the organic film.<sup>25,26</sup> The average concentrations of SO<sub>4</sub><sup>2-</sup> and NO<sub>3</sub><sup>-</sup> were reported to be 7.6 and 1.5 μg cm<sup>-2</sup>, respectively.<sup>26</sup>

Nitrate photolysis on grime, airborne particles, and other environmental surfaces has been suggested to produce nitrogen compounds such as NO, NO<sub>2</sub>, and HONO.<sup>23,27,28</sup> It has also been suggested that light-induced heterogeneous processing of NO<sub>2</sub> on simulated urban grime represents a source of HONO

Received: February 12, 2021

Revised: May 20, 2021

Accepted: May 21, 2021

Published: June 4, 2021



in the metropolitan area.<sup>23,29–32</sup> Recently, it has been shown that light-enhanced NO<sub>2</sub> uptake on real urban grime gives high HONO yields, which are largely dependent on the relative humidity (RH%).<sup>24</sup> Indeed, light intensity, RH, temperature (*T*), and NO<sub>2</sub> concentrations all impact the NO<sub>2</sub> uptake and the HONO formation yields on various environmental surfaces.<sup>24,33–41</sup>

To date, there have been no studies reported on the kinetics or the formation of HONO upon the reaction of NO<sub>2</sub> with OA. In this study, for the first time, to our best knowledge, we investigate the influence of RH% and light intensity on the heterogeneous reaction of NO<sub>2</sub> with an organic film consisting of (i) oleic acid (OA), (ii) a mixture of OA and sodium sulfate (Na<sub>2</sub>SO<sub>4</sub>), and (iii) a mixture of OA and sodium nitrate (NaNO<sub>3</sub>). The study was carried out in a well-established flow tube reactor, simultaneously coupled to a NO<sub>x</sub> analyzer to follow the NO<sub>2</sub> decay and to a membrane inlet single-photon ionization time-of-flight mass spectrometer (MI-SPI-TOFMS) for online measurements of the secondarily formed volatile organic compounds (VOCs). The HONO yields were detected indirectly with a coated Na<sub>2</sub>CO<sub>3</sub> denuder.

We show that the NO<sub>2</sub> uptake coefficients on solid OA films decrease as a function of RH. The presence of Na<sub>2</sub>SO<sub>4</sub> and NaNO<sub>3</sub> suppresses NO<sub>2</sub> reactivity but, yet, the increase of RH leads to an increase in the NO<sub>2</sub> uptake on OA/Na<sub>2</sub>SO<sub>4</sub> and OA/NaNO<sub>3</sub> mixtures. The reaction pathway of HONO and the nitroaromatic compound formation are discussed.

## MATERIALS AND METHODS

The film preparation, ion analysis, and UV–vis absorption measurements are given in the Supporting Information (SI).

The flow tube reactor used to assess the reaction of NO<sub>2</sub> with the coated glass plates has been previously detailed,<sup>24,42,43</sup> and in the SI only a brief description is given.

**NO<sub>x</sub> and HONO Measurements.** A saturated sodium carbonate (Na<sub>2</sub>CO<sub>3</sub>) solution was inserted into the denuder and allowed to stand for more than half an hour. Then, the denuder was wrapped in a tin foil and placed in an oven at about 106°C for drying. In this way, the denuder wall was coated with sodium carbonate crystals that are able to trap HONO (*vide infra*).

A NO<sub>2</sub> analyzer (Eco Physics, model CLD 88p) hyphenated with a photolytic (metal halide lamp) converter (Eco Physics, model PLC 860) was used to measure the NO<sub>x</sub> signal at the end of the flow tube reactor. The limit of detection of the NO<sub>x</sub> analyzer was 10 ppt with a time resolution of 1 s.<sup>24</sup>

The NO<sub>x</sub> analyzer uses a chemiluminescence method to measure the NO<sub>2</sub> concentration by converting NO<sub>2</sub> into NO with a molybdenum converter. With this method, one can directly measure NO without using the converter and NO<sub>x</sub> = NO + NO<sub>2</sub> when the converter is operational, thus obtaining NO<sub>2</sub> as the difference between the two signals. HONO will also be converted to NO, and thus, it has the same analytical response as NO<sub>2</sub>. The same NO<sub>x</sub> analyzer was used to simultaneously measure NO<sub>2</sub> (directly) and HONO<sup>33,34,37,44–46</sup> (indirectly as described in the SI).

**Membrane Inlet Single-Photon Ionization Time-of-Flight Mass Spectrometry (MI-SPI-TOFMS).** Membrane inlet single-photon ionization time-of-flight mass spectrometry (MI-SPI-TOFMS) is a promising technique for the online monitoring of VOCs. A commercial MI-SPI-TOF-MS device (SPIMS 3000, Guangzhou Hexin Instrument Co., Ltd., China) was used in this study for real-time monitoring of the gaseous

product compounds generated by the reaction of NO<sub>2</sub> with OA, OA/NaNO<sub>3</sub>, or OA/Na<sub>2</sub>SO<sub>4</sub>. The details of this instrument are given elsewhere<sup>47–49</sup> and here only a short description is given. Briefly, SPIMS 3000 consists of three parts: (1) a membrane inlet system, with porous membrane consisting of dimethylsiloxane (PDMS) with a thickness of 0.002 in. (Technical Production, Inc.) that serves to enrich the VOCs; (2) a single-photon ionization (SPI) source, which uses a commercial deuterium lamp (Hamamatsu, Japan), and (3) a reflectron TOF-MS, containing a double-pulsed acceleration region, a field-free drift tube, a reflector, and an ion detector.<sup>47</sup> The raw data were analyzed by software (SPIMS 3000 V1.0.1.2.0, Guangzhou Hexin Instrument Co., Ltd., China), whereas selected Gauss peaks above a predetermined threshold are rounded with an average value.<sup>47–49</sup>

**Treatment of the Uptake Coefficients.** The reactive uptakes of NO<sub>2</sub> ( $\gamma_{\text{NO}_2}$ ) on the coated glass plates were estimated as follows:

$$\gamma_{\text{NO}_2} = \frac{4 k_{1,\text{NO}_2} V}{\nu_{\text{NO}_2} S} \quad (1)$$

where  $k_{1,\text{NO}_2}$  is the determined pseudo-first-order rate constant for the reaction between NO<sub>2</sub> and the glass plate coated with either OA, OA/NaNO<sub>3</sub>, or OA/Na<sub>2</sub>SO<sub>4</sub>,  $\nu_{\text{NO}_2}$  is the relative mean speed of gaseous NO<sub>2</sub>, *S* is the reactive surface of the glass plate, and *V* is the volume of the flow tube.<sup>24</sup> The estimation of  $k_{1,\text{NO}_2}$  is described in the SI.

We performed test experiments in the empty reactor to check for photodissociation of NO<sub>2</sub> and the formation of ozone.<sup>50,51</sup> Indeed, the lamps used in this study irradiate in the wavelength region between 300 and 400 nm, which can cause photolysis of NO<sub>2</sub>. The photolysis rate of NO<sub>2</sub> ( $J(\text{NO}_2)$ ) in the flow tube ranged from  $9.5 \times 10^{-5}$  to  $3.2 \times 10^{-4} \text{ s}^{-1}$ , which implies only slight photodissociation of NO<sub>2</sub> (accounting for 0.1 to 0.4% of the total NO<sub>2</sub>). The connected ozone analyzer at the exit of the reactor did not detect any ozone, which could eventually be formed by the photolysis of NO<sub>2</sub>.

## RESULTS AND DISCUSSION

**Effect of RH.** The uptake coefficients of NO<sub>2</sub> on oleic acid were assessed as a function of RH at 296 K (Figure 1). The NO<sub>2</sub> uptakes decreased linearly with the increase of RH, from  $(1.4 \pm 0.1) \times 10^{-6}$  at 0% RH to  $(7.1 \pm 1.6) \times 10^{-7}$  at 90% RH, under light irradiation ( $15.5 \text{ W m}^{-2}$ ,  $5.3 \times 10^{13} \text{ photons cm}^{-2} \text{ s}^{-1}$ ;  $300 \text{ nm} < \lambda < 400 \text{ nm}$ ).

The NO<sub>2</sub> uptake on OA at 0% RH was slightly higher than the reactive uptake reported for NO<sub>2</sub> on real urban grime ( $\gamma(\text{NO}_2) = (1.1 \pm 0.2) \times 10^{-6}$  at 0% RH).<sup>24</sup> Although the NO<sub>2</sub> uptake values decreased with RH, the value  $\gamma(\text{NO}_2) = (1.2 \pm 0.1) \times 10^{-6}$  observed at 30% RH was still about 2 times higher than the reactive uptake reported for NO<sub>2</sub> on fluoranthene/KNO<sub>3</sub> ( $\gamma(\text{NO}_2) = 6.6 \times 10^{-7}$  at 35% RH) and phenanthrene/KNO<sub>3</sub> ( $\gamma(\text{NO}_2) = 7.8 \times 10^{-7}$  at 35% RH).<sup>33</sup>

The decrease of NO<sub>2</sub> uptake values with increasing RH observed here is completely opposite to the dependence of the NO<sub>2</sub> uptake values on fluorene (FL) and FL/Na<sub>2</sub>SO<sub>4</sub>, where a nonlinear increase of NO<sub>2</sub> uptake was observed with increasing RH.<sup>43</sup>

Considering that OA is poorly soluble in water, when RH increases, the formation of a water layer may occur above OA that reduces the accessibility of NO<sub>2</sub> to the adsorption sites on

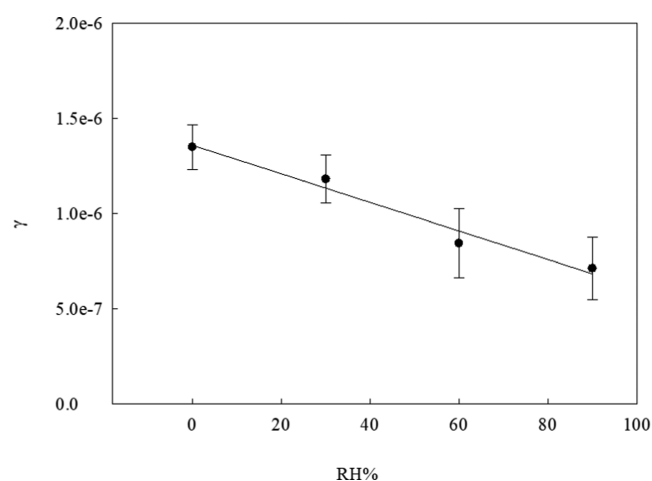


**Figure 1.**  $\text{NO}_2$  uptake coefficients on (●) OA as a function of RH at a  $\text{NO}_2$  mixing ratio of 40 ppb and under light irradiation ( $15.5 \text{ W m}^{-2}$ ,  $5.3 \times 10^{13} \text{ photons cm}^{-2} \text{ s}^{-1}$ ;  $300 \text{ nm} < \lambda < 400 \text{ nm}$ ) at 296 K. The error bars are estimated from the uncertainties related to the calculation of the uptake coefficients.

OA. Considering that the melting point of OA is 288 K, the OA film is expected to be liquid at 296 K. Therefore, most likely, reversible adsorption of water occurs on liquid OA and leads to displacement or competition for adsorption with  $\text{NO}_2$ .

If this is the case, at 90% RH, the measured uptake coefficient of  $\text{NO}_2$  on OA should correspond to the uptake coefficient of  $\text{NO}_2$  on a water layer. To verify this hypothesis, we measured the  $\text{NO}_2$  uptake coefficients on a clean glass plate at 90% RH in the absence of any organics. The uptake coefficient obtained in these conditions was  $(7.6 \pm 0.5) \times 10^{-7}$ , which is similar to the  $\text{NO}_2$  uptake of  $(7.1 \pm 1.6) \times 10^{-7}$  measured on the OA film at 90% RH, and implies that OA is not accessible for  $\text{NO}_2$  at 90% RH.

The addition to OA with  $\text{Na}_2\text{SO}_4$  and  $\text{NaNO}_3$  inhibited substantially the uptake of  $\text{NO}_2$  at 0% RH: it passed from  $\gamma(\text{NO}_2) = (1.4 \pm 0.1) \times 10^{-6}$  without salts to  $\gamma(\text{NO}_2) = (7.7 \pm 1.7) \times 10^{-7}$  with  $\text{Na}_2\text{SO}_4$ , and  $\gamma(\text{NO}_2) = (4.7 \pm 2.4) \times 10^{-7}$  with  $\text{NaNO}_3$ . Conversely, the uptake coefficient of  $\text{NO}_2$  on a mixture OA/ $\text{Na}_2\text{SO}_4$  was  $(1.5 \pm 0.5) \times 10^{-6}$  at 90% RH, which is similar to  $\gamma(\text{NO}_2) = (1.4 \pm 0.1) \times 10^{-6}$  on OA at 0% RH. Indeed, increasing RH led to an increase of the  $\text{NO}_2$  uptake values on both films, OA/ $\text{Na}_2\text{SO}_4$  and OA/ $\text{NaNO}_3$  (Figure 2).

The obtained  $\text{NO}_2$  uptake coefficients on OA/ $\text{NaNO}_3$  in the dark (Figure 2) are very similar to those observed under irradiation, which could be ascribed to the light-absorbing properties of OA/ $\text{NaNO}_3$  and to the spectral irradiance emitted by the lamps. Namely, Figure S1 shows that the absorption spectrum of OA/ $\text{NaNO}_3$  only slightly overlaps with the emission spectrum of the lamps in the near-UV region ( $300 \text{ nm} < \lambda < 400 \text{ nm}$ ).

Considering that the deliquescent RH for  $\text{NaNO}_3$  particles is 74.5%,<sup>52</sup> the binary system OA/ $\text{NO}_3^-$  is in a relatively dry state. In the presence of  $\text{NO}_3^-$  ions, at RH higher than 74.5%, the liquid film becomes deliquesced. Therefore, it is most likely that at  $\text{RH} > 74.5\%$ , the salting-out effect makes OA more accessible for the reaction with  $\text{NO}_2$ . A salting-out effect has been previously observed for the reactions of ozone ( $\text{O}_3$ ) with acetosyringone<sup>53</sup> and pyruvic acid<sup>54</sup> in the presence of  $\text{SO}_4^{2-}$  and  $\text{Br}^-$ , respectively.

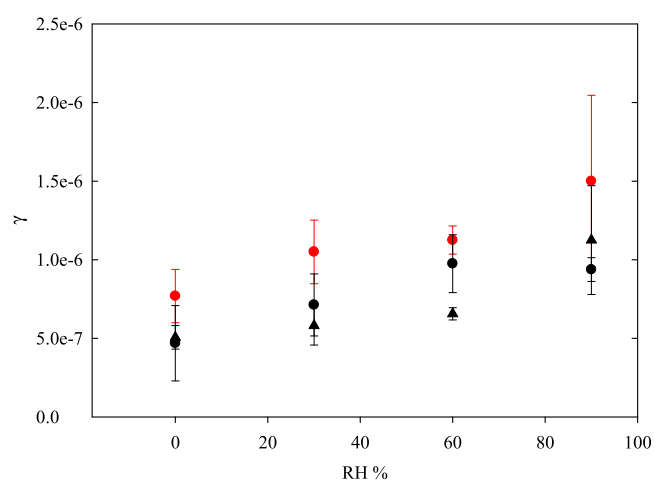


**Figure 2.**  $\text{NO}_2$  uptake coefficients on (●) OA/ $\text{NaNO}_3$  and (red solid circle) OA/ $\text{Na}_2\text{SO}_4$ , as a function of RH at a  $\text{NO}_2$  mixing ratio of 40 ppb, and light irradiation ( $15.5 \text{ W m}^{-2}$ ,  $5.3 \times 10^{13} \text{ photons cm}^{-2} \text{ s}^{-1}$ ;  $300 \text{ nm} < \lambda < 400 \text{ nm}$ ) at 296 K.  $\text{NO}_2$  uptake coefficients on (▲) OA/ $\text{NaNO}_3$  under dark conditions. The error bars are estimated from the uncertainties related to the calculation of the uptake coefficients.

**Effect of Light Intensity.** The effect of light intensity on the  $\text{NO}_2$  uptake coefficients measured on OA, OA/ $\text{Na}_2\text{SO}_4$ , and OA/ $\text{NaNO}_3$  was also evaluated. The uptake coefficients of  $\text{NO}_2$  on OA were almost independent of light intensity and ranged between  $(5.6 \pm 0.9) \times 10^{-7}$  at  $4.1 \text{ W m}^{-2}$  and  $(6.9 \pm 0.6) \times 10^{-7}$  at  $15.5 \text{ W m}^{-2}$  (Figure 3).

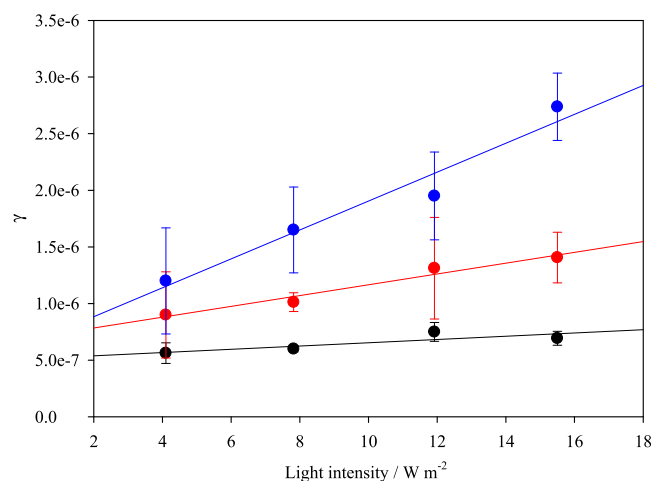


**Figure 3.**  $\text{NO}_2$  uptake coefficients on (●) OA, (red solid circle) OA/ $\text{Na}_2\text{SO}_4$ , and (blue solid circle) OA/ $\text{NaNO}_3$  as a function of the photon flux, at a  $\text{NO}_2$  mixing ratio of 40 ppb with 40% RH at 296 K. The error bars are estimated from the uncertainties related to the calculation of the uptake coefficients. The black, red, and blue lines represent the regression lines for the dependence of  $\text{NO}_2$  uptake coefficients on OA, OA/ $\text{Na}_2\text{SO}_4$ , and OA/ $\text{NaNO}_3$ , respectively.

When OA was mixed with  $\text{Na}_2\text{SO}_4$ , the  $\text{NO}_2$  uptake coefficients slightly increased from  $(9.0 \pm 3.8) \times 10^{-7}$  at  $4.1 \text{ W m}^{-2}$  to  $(1.4 \pm 0.2) \times 10^{-6}$  at  $15.5 \text{ W m}^{-2}$ . In contrast, in the case of OA +  $\text{NaNO}_3$  simultaneously exposed to  $\text{NO}_2$  and light, there was a significant increase in the  $\text{NO}_2$  uptake coefficients by a factor of about 2 (Figure 3), from  $(1.2 \pm 0.5) \times 10^{-6}$  at  $4.1 \text{ W m}^{-2}$  to  $(2.7 \pm 0.3) \times 10^{-6}$  at  $15.5 \text{ W m}^{-2}$ . This latter finding could be ascribed to the increased overlap of the



**Table 1. Formation Yields of HONO and NO in Dark and under Light Irradiation (15.5 W m<sup>-2</sup>) with Different RH Values, at 40 ppb of NO<sub>2</sub> and 293 K**

RH %	oleic acid				oleic acid + Na <sub>2</sub> SO <sub>4</sub>				oleic acid + NaNO <sub>3</sub>			
	dark		light		dark		light		dark		light	
	HONO yield%	NO yield%	HONO yield%	NO yield%	HONO yield%	NO yield%	HONO yield%	NO yield%	HONO yield%	NO yield%	HONO yield%	NO yield%
0	11.8	4.8	17.2	9.2	18.5	7.7	28.7	8.4	62.2	15.2	44.5	10.6
30	15.9	0.5	31.9	22.5	15.6	7.7	19.7	6.4	25.5	3.8	30.4	10.4
60	25.9	5.1	28.1	9.2	13.9	6.0	25.7	4.0	47.4	9.5	49.0	5.6
90	26.0	3.3	30.8	8.8	30.6	2.0	27.8	4.1	36.5	4.5	40.3	24.6

emission spectrum of 3 and 4 UV lamps with the absorption spectrum of OA/NaNO<sub>3</sub> (Figure S1).

From the regression line of the plot of  $\gamma$  versus light intensity, eq 2 is obtained that can be used to predict the reactive uptake of NO<sub>2</sub> on OA/NaNO<sub>3</sub> under realistic light intensity, which is here expressed in W m<sup>-2</sup> in the near-UV region of the solar spectrum (300 nm <  $\lambda$  < 400 nm) at different solar zenith angles (SZA).

$$\gamma = (6.3 \pm 2.2) \times 10^{-7} + (1.3 \pm 0.2) \times 10^{-7} \cdot \text{light intensity} / \text{W m}^{-2}$$

$$r^2 = 0.99 \quad (2)$$

It is interesting to compare, with previous studies, the extrapolated NO<sub>2</sub> uptake coefficient on a film consisting of OA/NaNO<sub>3</sub>, at a UV radiation intensity of 46 W m<sup>-2</sup> for the wavelength range 300–400 nm corresponding to a solar zenith angle of 48° (National Renewable Energy Laboratory (NREL)<sup>55</sup>), which would be  $\gamma = 6.6 \times 10^{-6}$ . This value is of the same order of magnitude as the uptake of NO<sub>2</sub> on pyrene<sup>29</sup> ( $\gamma = 8.8 \times 10^{-6}$  at 50 ppb of NO<sub>2</sub>), and is about 4 times higher than the uptake of NO<sub>2</sub> on simulated soot made up of gentisic acid ( $\gamma = 1.6 \times 10^{-6}$ , obtained at a NO<sub>2</sub> mixing ratio of 20 ppb and 20% RH, under UV–vis light irradiation at 40° solar zenith angle).<sup>32</sup> The uptake of NO<sub>2</sub> (20 ppb) on fluoranthene,  $\gamma = 1 \times 10^{-6}$ ,<sup>33</sup> was about 7 times lower than the uptake of NO<sub>2</sub> on OA/NaNO<sub>3</sub> as determined in this study ( $\gamma = 6.6 \times 10^{-6}$ ). Moreover, our latter value ( $6.6 \times 10^{-6}$ ) is 1.5 times lower than the NO<sub>2</sub> uptake on a solid film of fluorene, obtained at a NO<sub>2</sub> mixing ratio of 40 ppb and 60% RH, under a light intensity of 46 W m<sup>-2</sup> for  $\lambda = 300$ –400 nm.<sup>43</sup> Our value is also 1.5 times lower than the uptake coefficient of NO<sub>2</sub> measured on a simulated soil surface consisting of humic acid ( $\gamma = 1 \times 10^{-5}$ ) under an irradiation intensity of 400 W m<sup>-2</sup>, in the visible range of wavelengths ( $\lambda = 400$ –700 nm) at 48° solar zenith angle, with a NO<sub>2</sub> mixing ratio of 30 ppb,  $T = 298$  K, and 30% RH.<sup>34</sup>

The extrapolated NO<sub>2</sub> uptake coefficient (eq 3) on an OA/Na<sub>2</sub>SO<sub>4</sub> film under the same irradiation conditions would be  $\gamma = 2.9 \times 10^{-6}$ , which is about 2 times lower than the value of  $\gamma$  on OA/NaNO<sub>3</sub>, but still ca. 3 times higher than the NO<sub>2</sub> uptakes on gentisic acid,  $\gamma = 1.6 \times 10^{-6}$ , and on fluoranthene,  $\gamma = 1 \times 10^{-6}$ .<sup>32,33</sup> With OA/Na<sub>2</sub>SO<sub>4</sub> one gets the following equation

$$\gamma = (6.9 \pm 0.7) \times 10^{-7} + (4.8 \pm 0.6) \times 10^{-8} \cdot \text{light intensity} / \text{W m}^{-2}$$

$$r^2 = 0.96 \quad (3)$$

Finally, the extrapolated NO<sub>2</sub> uptake coefficient on a film containing only pure OA (eq 4) under the same irradiation conditions would be  $1.2 \times 10^{-6}$ , which falls in the range of the NO<sub>2</sub> uptakes on gentisic acid,  $\gamma = 1.6 \times 10^{-6}$ ,<sup>32</sup> and fluoranthene,  $\gamma = 1 \times 10^{-6}$ .<sup>33</sup>

$$\gamma = (5.1 \pm 0.7) \times 10^{-7} + (1.4 \pm 0.7) \times 10^{-8} \cdot \text{light intensity} / \text{W m}^{-2}$$

$$r^2 = 0.7 \quad (4)$$

Considering that in the UV range of wavelengths, the light flux in the indoor environment is 9 W m<sup>-2</sup>,<sup>56</sup> the interpolated NO<sub>2</sub> uptake coefficients would be  $1.8 \times 10^{-6}$ ,  $1.1 \times 10^{-6}$ , and  $6.4 \times 10^{-7}$  in the cases of OA/NaNO<sub>3</sub>, OA/Na<sub>2</sub>SO<sub>4</sub>, and OA, respectively. Although these uptakes are relatively low when compared to the corresponding values obtained for urban grime under a UV light intensity of 46 W m<sup>-2</sup> (see above), the observed HONO yields generated by NO<sub>2</sub> conversion on OA/NaNO<sub>3</sub>, OA/Na<sub>2</sub>SO<sub>4</sub>, and OA (*vide infra*) can have health implications for the inhabitants who inhale HONO.<sup>57,58</sup> Moreover, HONO photolysis and the associated production of hydroxyl radicals (OH) may play a key role in the formation of toxic secondary compounds in urban and indoor air.<sup>11,48,59–62</sup>

**Comparison between Spectral Irradiance and UV Absorption Spectra.** To understand the dependence of the uptake coefficients on the light intensity (Figure 3), we measured the spectral irradiance of the four UV lamps used to irradiate the glass plates in our flow tube reactor and compared it with the UV–vis absorption spectra of the coated (OA, OA/Na<sub>2</sub>SO<sub>4</sub>, OA/NaNO<sub>3</sub>) glass plates (Figure S1).

Figure S1 shows only a slight overlap of spectral irradiance with UV absorption spectra when one or two UV lamps were used. This is the most likely reason for the very similar values of the NO<sub>2</sub> uptake coefficients measured on OA/NaNO<sub>3</sub>, in the dark and under irradiation with two lamps (Figure 2). By increasing the number of lamps, one has a stronger overlap between the film absorption spectra and the lamp spectral irradiance, which may explain the increase of the uptake coefficients with the light intensity shown in Figure 3, especially in the case of OA/NaNO<sub>3</sub>.

It is known that nitrates can absorb UVB as well as short-wavelength UVA radiation and produce HONO after the photodissociation process.<sup>27,28</sup> The photolysis rate of HNO<sub>3</sub> adsorbed on borosilicate glass (the same material as the glass plates used in this study) has been reported as  $1.2 \times 10^{-5} \text{ s}^{-1}$  at 50% RH, which is two orders of magnitude higher compared to liquid-phase and gas-phase HNO<sub>3</sub> under comparable irradiation conditions.<sup>27</sup> Moreover, solid nitrate near the surface does not undergo the solvent-cage effect that is experienced in aqueous solutions, where photogenerated OH + NO<sub>2</sub> are

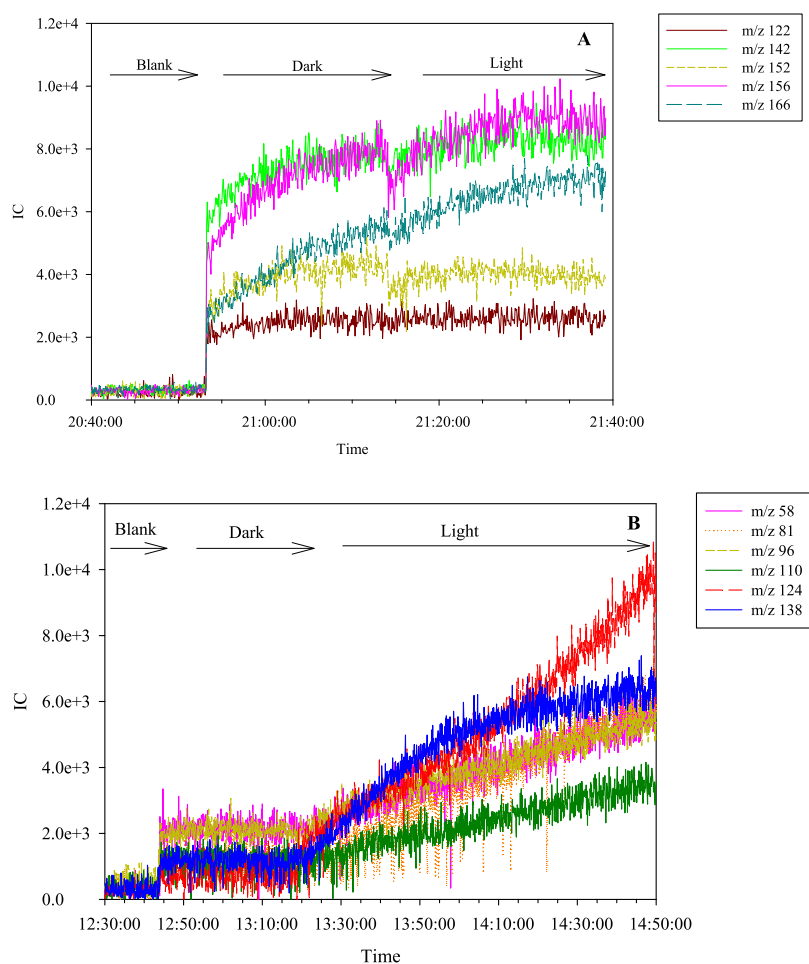


**Figure 4.** Typical profiles of gas-phase compounds formed upon heterogeneous reactions of  $\text{NO}_2$  with (A) OA and (B)  $\text{OA}/\text{NaNO}_3$ .

initially surrounded by a cage of water molecules that favor the recombination to  $\text{NO}_3^- + \text{H}^+$  at the expense of diffusion of OH and  $\text{NO}_2$  into the solution bulk. Indeed, the solvent-cage effect decreases the net rate of  $\text{NO}_3^-/\text{HNO}_3$  photolysis in the solution (*vide infra*).<sup>63</sup>

**HONO and  $\text{NO}$  Yields.** When the  $\text{NO}_x$  analyzer was directly hyphenated to the flow tube reactor, a decrease of the  $\text{NO}_2$  signal was observed due to the uptake of  $\text{NO}_2$  by the OA film. When the  $\text{Na}_2\text{CO}_3$  denuder was connected between the flow tube reactor and the  $\text{NO}_x$  analyzer, an additional decrease of the  $\text{NO}_2$  signal was observed that corresponds to the HONO trapped by the denuder. The HONO mixing ratio was obtained as the difference between the  $\text{NO}_2$  signals without and with the  $\text{Na}_2\text{CO}_3$  denuder.

The HONO and  $\text{NO}$  yields produced by light-induced heterogeneous reaction of  $\text{NO}_2$  with films containing OA,  $\text{OA}/\text{Na}_2\text{SO}_4$ , and  $\text{OA}/\text{NaNO}_3$  were calculated as the ratios  $\Delta\text{HONO}/\Delta\text{NO}_2$  and  $\Delta\text{NO}/\Delta\text{NO}_2$ , respectively (Table 1). Table 1 shows that the HONO and  $\text{NO}$  yields only slightly varied with the RH. The most efficient conversion of  $\text{NO}_2$  to HONO was observed with  $\text{OA}/\text{NaNO}_3$  in the dark, with HONO yields ranging from 26% at 30% RH to 62% in the absence of RH. Under light irradiation, the most efficient HONO formation was also observed with  $\text{OA}/\text{NaNO}_3$ , with HONO yields ranging from 30% at 30% RH to 49% at 60% RH. This finding suggests that nitrate promotes the conversion process of  $\text{NO}_2$  to HONO on the fatty acid surface (Table 1).

Table S7 shows the effect of nitrate ions on HONO formation, in the dark and under light irradiation. It can be seen from Table S7 that the quantity of HONO ( $\Delta\text{HONO}$ ) formed upon reaction of  $\text{NO}_2$  with  $\text{OA}/\text{NaNO}_3$  under light irradiation is higher than that in dark, especially at high RH. At the same time, however,  $\text{NO}_2$  uptake increased as well and the overall HONO yield was almost unchanged. It can also be seen that the formed amount of HONO, during the light-induced reaction of  $\text{NO}_2$  with  $\text{OA}/\text{NaNO}_3$ , increases with increasing RH. The ion chromatography analysis revealed that the quantity of  $\text{NO}_3^-$  at 60% RH increased from 9 ppm before the reaction to, respectively, 24 and 22 ppm after 1 h of heterogeneous reaction of  $\text{NO}_2$  with  $\text{OA}/\text{NaNO}_3$ , in the dark and under irradiation. These results suggest that at 60% RH, 49% of  $\text{NO}_2$  was converted into gaseous HONO but the remaining  $\approx 50\%$  was converted into nitric acid ( $\text{HNO}_3$ ), which remained on the flow tube surface. The quantity of  $\text{NO}_2^-$  only slightly increased, from 0 ppm before the reaction to 0.067 and 0.008 ppm following the reaction of  $\text{NO}_2$  with  $\text{OA}/\text{NaNO}_3$ , respectively, in the dark and under irradiation. The amounts of  $\text{NO}_3^-$  and  $\text{NO}_2^-$  ions also increased from 2 to 5 ppm and from 0.017 to 0.027 ppm, respectively, after 1 h light-induced heterogeneous reaction of  $\text{NO}_2$  with the OA film. Intriguingly, the quantity of  $\text{NO}_3^-$  and  $\text{NO}_2^-$  ions decreased from 0.003 to 0 ppm and from 0.04 to 0.006 ppm, respectively, after 1 h reaction of  $\text{NO}_2$  with the film consisting of  $\text{OA}/\text{Na}_2\text{SO}_4$  in the presence of light.

**Gas-Phase Product Compounds Detected by MI-SPI-TOFMS Analysis.** The formation of gaseous compounds released upon heterogeneous reactions of NO<sub>2</sub> with OA, OA/NaNO<sub>3</sub>, and OA/Na<sub>2</sub>SO<sub>4</sub> at 30% RH, in the dark and under irradiation was monitored online by MI-SPI-TOF-MS. The increase of RH to 90% substantially reduced the total ion counts of the gas-phase compounds observed with NO<sub>2</sub> + OA (Figure S2), thereby confirming our hypothesis that at higher RH, OA is covered with a water layer that both inhibits the reaction and leads to lower NO<sub>2</sub> uptake values (Figure 1).

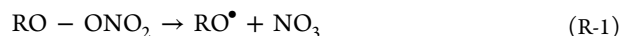
Figures S4–S6 show the signal intensities obtained from scans of mass-to-charge ratios (*m/z*) ranging between 50 and 250 amu, which are relevant to the observed gas-phase compounds formed upon reaction of NO<sub>2</sub> with OA, OA/NaNO<sub>3</sub>, and OA/Na<sub>2</sub>SO<sub>4</sub>, in the dark and under irradiation with simulated sunlight, at 30% RH. The main differences that can be observed are related to the presence of either NaNO<sub>3</sub> or Na<sub>2</sub>SO<sub>4</sub> on the film consisting of OA. Namely, the presence of NO<sub>3</sub><sup>−</sup> promotes the formation of N-containing organic compounds (see the Reaction Mechanism section), and the presence of SO<sub>4</sub><sup>2−</sup> increases substantially the number of the formed compounds. Tables S1–S3 summarize all the detected *m/z* values under different conditions, showing that the highest abundances occurred with OA/Na<sub>2</sub>SO<sub>4</sub>, both in the dark and under irradiation.

It can be seen from Figures S4–S6 that certain product peaks are separated by  $\Delta m/z = 16$ , which corresponds to multiple additions of O atoms that suggest the formation of carbonyl compounds and alcohols.<sup>21</sup> The oxidation of the saturated alkyl groups is in fact associated with an addition of 14 Da (carbonyl) and then by the 16 Da (hydroxyl) pattern (Figures S4–S6).<sup>64</sup>

Figure 4 shows typical profiles for the formation of gas-phase compounds upon the reaction of NO<sub>2</sub> with OA and OA/NaNO<sub>3</sub>, in the dark and under irradiation. The variation trend of five compounds (*m/z* 122, 142, 152, 156, and 166) formed upon heterogeneous reactions of NO<sub>2</sub> with OA is shown in Figure 4A. The profiles of these five products were very similar in the dark and in the presence of light. However, the presence of nitrate ions in the OA film suppressed the formation of VOCs in the dark (Table S2) but induced the formation of several new compounds (*m/z* 58, 81, 96, 110, 124, and 138) under irradiation (Figure 4B). The MS data suggest that the latter compounds likely bear nitro groups. This finding indicates that the NO<sub>3</sub><sup>−</sup> ions favor the formation of secondary nitro-organics as well as HONO, which would be released upon light-induced NO<sub>2</sub> reactions with OA. Figure S3 shows that the total ion current (TIC) at different *m/z* values slightly decreased with increasing RH (from 30 to 90% in the dark) but then increased again to the initial level upon light irradiation of OA/NaNO<sub>3</sub> at 90% RH. When sulfate ions were present in the OA film, most of the gas-phase compounds were formed in the dark (Figure S4). Compared to the gas-phase compounds formed by the reaction of NO<sub>2</sub> with OA and the OA/NaNO<sub>3</sub> surface, there were three distinct compounds (*m/z* 100, 188, 216) formed upon the dark heterogeneous reaction of NO<sub>2</sub> with OA/Na<sub>2</sub>SO<sub>4</sub> (Figure S7 and Table S3). In addition, there are some compounds, the intensities of which increase under light irradiation (*m/z* 57, 81, 124, 138) (Figure S7).

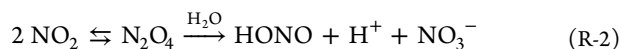
**Reaction Mechanism.** Unsaturated fatty acids such as OA contain double bonds, which are susceptible to NO<sub>2</sub> attack via either homolytic or heterolytic (ionic) reactions. Hydrogen

(H) atom abstraction might also occur at the bis-allylic methylene center of OA, which leads to the formation of pentadienyl radicals.<sup>65</sup> The initial product compounds of H-abstraction by NO<sub>2</sub> from OA would be HONO and a resonance-stabilized allylic radical,<sup>66</sup> but H-abstraction is too slow to compete with NO<sub>2</sub> addition to the double bond.<sup>67</sup> Nevertheless, in the presence of O<sub>2</sub>, alkoxy radicals could be formed through dissociation of peroxy nitrates, as follows.<sup>68</sup>



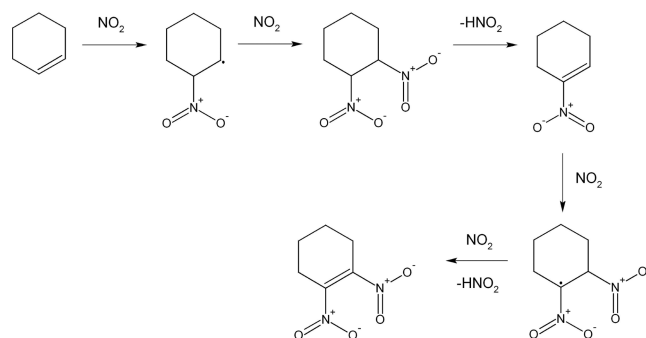
The formed alkoxy radicals could abstract the H-atom from cyclohexene (*m/z* 82) to produce 2-cyclohexenol (*m/z* 98) (Tables S1–S3).<sup>67</sup>

The reaction of NO<sub>2</sub> with OA proceeds through fast and reversible addition of NO<sub>2</sub> to alkene double bonds to initially form  $\beta$ -nitroalkyl radicals.<sup>67</sup> The reaction of the  $\beta$ -nitroalkyl radical with another NO<sub>2</sub> molecule might then proceed through H-abstraction, which would yield nitro-OA and HONO. This process, which can also take place in the dark, would produce HONO with 50% yield and might significantly contribute to HONO production, especially at low RH (Table 1). At the same time, nonvolatile nitro-OA would remain attached to the film and would not contribute to the observed nitrated VOCs. In contrast, the formation of 50% HONO + 50% HNO<sub>3</sub> that was observed at 60% RH is consistent with the well-known hydrolysis pathway of NO<sub>2</sub> in the presence of a liquid phase



One of the gaseous products formed by NO<sub>2</sub> addition to the C=C bond is 1,2-dinitrocyclohexene (*m/z* 174),<sup>67</sup> which was also tentatively identified in this study (Tables S1 and S3). A tentative reaction pathway leading to the formation of this compound, assuming cyclohexene as the precursor, is provided in Scheme 1. Interestingly, the proposed addition–elimination

#### Scheme 1. Proposed Reaction Pathway for the Formation of the Tentatively Detected Compound 1,2-Dinitrocyclohexene<sup>a</sup>



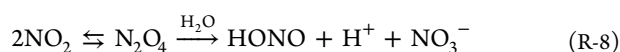
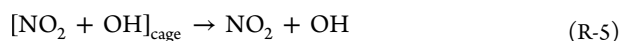
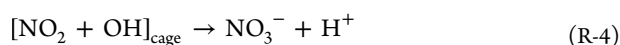
<sup>a</sup>Here, we assume that cyclohexene derives from OA fragmentation.

pathway is exactly the opposite as the nitration of phenolic compounds by NO<sub>2</sub>, which first proceeds via H-abstraction to produce HONO and a phenoxy radical, followed by NO<sub>2</sub> addition to finally produce the nitrophenol.<sup>69</sup>

The relatively high HONO values formed at high RH in the presence of OA/NaNO<sub>3</sub> under irradiation (Table S7) could be accounted for by an additional process, yielding HONO from the photochemistry of nitrate. Indeed, liquid-phase NO<sub>3</sub><sup>−</sup> is a significant photochemical source of NO<sub>2</sub><sup>−</sup> and of the gas-phase

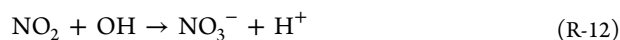


HONO as a consequence (see the reaction sequence from reaction R-3 to R-9).<sup>70</sup>



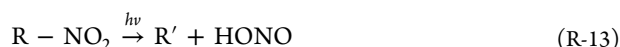
where  $\text{OA}_{\text{ox}}$  is a radical species arising from the OH addition to OA. The formation of OA as an OH scavenger could enhance the photoproduction of HONO by inhibiting the recombination between the geminate species produced by nitrate photolysis inside the solvent cage.<sup>63</sup> The photogeneration of OH by photolysis of nitrate and possibly of photogenerated  $\text{NO}_2^-$  and HONO (reactions R-10 and R-11)<sup>69</sup> could significantly contribute to the occurrence of oxidized/hydroxylated compounds.

At the same time, however, the hydroxyl radicals produced under irradiation could cause  $\text{NO}_2$  oxidation and enhance its conversion (reaction R-12). Indeed, although a significant part of OH would be scavenged by OA, reaction R-12 cannot occur in the dark as no OH is generated in such conditions. Therefore, it is reasonable for  $\text{NO}_2$  conversion to be faster under irradiation than in the dark.



The increase in both HONO production and  $\text{NO}_2$  processing might explain why the HONO yield changed very little with  $\text{NaNO}_3$  in the dark or under irradiation (Table 1), despite the increased production of HONO under irradiation (Table S7).

Interestingly, the photolysis of the formed N-containing compounds such as 1,2-dinitrocyclohexene (Scheme 1) can be plausibly linked with HONO formation, as shown by reaction R-13, which can be an additional photochemical source of HONO in the metropolitan area.<sup>71–73</sup>



Considering that fatty acids are ubiquitous surfactants in the atmospheric particles and on urban and indoor grime, the obtained results suggest that fatty acids can contribute to urban- and indoor air pollution through heterogeneous conversion of  $\text{NO}_2$  into N-containing organic compounds. The detailed knowledge of HONO formation processes is paramount with respect to the urban and indoor air chemistry because HONO is the main source of OH radicals through its photolysis in the urban environment<sup>60–62</sup> and in sunlit areas of the indoor environment.<sup>48,59</sup> Especially, the formation of N-containing organic compounds by the reaction of  $\text{NO}_2$  with

the OA in the presence of nitrate ions can exhibit health problems. The presence of  $\text{NO}_3^-$  ions during the heterogeneous  $\text{NO}_2$  processing of OA stimulates the formation of nitroaromatic compounds, which are potential light-absorbing (brown carbon) compounds that could affect the climate through positive radiative forcing (warming).<sup>74</sup>

## ■ ASSOCIATED CONTENT

### Supporting Information

The Supporting Information is available free of charge at <https://pubs.acs.org/doi/10.1021/acs.est.1c01043>.

Film preparation; ion analysis; description of the flow tube reactor; estimation of the pseudo-first-order rate constant; indirect detection of HONO; comparison of the spectral irradiance of the UV lamps with the absorption spectra of OA, OA/ $\text{NaNO}_3$ , and OA/ $\text{Na}_2\text{SO}_4$ ; total ion count of the monitored gaseous compounds; the relative intensity of the observed  $m/z$ ; typical profiles of gas-phase compounds formed upon heterogeneous reactions of  $\text{NO}_2$  with OA/ $\text{Na}_2\text{SO}_4$ ; HONO and NO values and yields (PDF)

## ■ AUTHOR INFORMATION

### Corresponding Authors

**Sasho Gligorovski** – State Key Laboratory of Organic Geochemistry and Guangdong Provincial Key Laboratory of Environmental Protection and Resources Utilization, Guangzhou Institute of Geochemistry, Chinese Academy of Sciences, Guangzhou 510640, China; Guangdong-Hong Kong-Macao Joint Laboratory for Environmental Pollution and Control, Guangzhou Institute of Geochemistry and Center for Excellence in Deep Earth Science, Chinese Academy of Science, Guangzhou 510640, China; [orcid.org/0000-0003-4151-2224](https://orcid.org/0000-0003-4151-2224); Phone: +86 2085291497; Email: [gligorovski@gig.ac.cn](mailto:gligorovski@gig.ac.cn)

**Xue Li** – Institute of Mass Spectrometry and Atmospheric Environment, Jinan University, Guangzhou 510632, China; [orcid.org/0000-0001-9247-0584](https://orcid.org/0000-0001-9247-0584); Phone: +86 2085221076; Email: [tamylee@jnu.edu.cn](mailto:tamylee@jnu.edu.cn)

### Authors

**Huifan Deng** – State Key Laboratory of Organic Geochemistry and Guangdong Provincial Key Laboratory of Environmental Protection and Resources Utilization, Guangzhou Institute of Geochemistry, Chinese Academy of Sciences, Guangzhou 510640, China; University of Chinese Academy of Sciences, Beijing 100049, China

**Jiangping Liu** – State Key Laboratory of Organic Geochemistry and Guangdong Provincial Key Laboratory of Environmental Protection and Resources Utilization, Guangzhou Institute of Geochemistry, Chinese Academy of Sciences, Guangzhou 510640, China; University of Chinese Academy of Sciences, Beijing 100049, China

**Yiqun Wang** – State Key Laboratory of Organic Geochemistry and Guangdong Provincial Key Laboratory of Environmental Protection and Resources Utilization, Guangzhou Institute of Geochemistry, Chinese Academy of Sciences, Guangzhou 510640, China; University of Chinese Academy of Sciences, Beijing 100049, China

**Wei Song** – State Key Laboratory of Organic Geochemistry and Guangdong Provincial Key Laboratory of Environmental Protection and Resources Utilization, Guangzhou Institute of

Geochemistry, Chinese Academy of Sciences, Guangzhou 510640, China; Guangdong-Hong Kong-Macao Joint Laboratory for Environmental Pollution and Control, Guangzhou Institute of Geochemistry and Center for Excellence in Deep Earth Science, Chinese Academy of Science, Guangzhou 510640, China

**Xinming Wang** – State Key Laboratory of Organic Geochemistry and Guangdong Provincial Key Laboratory of Environmental Protection and Resources Utilization, Guangzhou Institute of Geochemistry, Chinese Academy of Sciences, Guangzhou 510640, China; Guangdong-Hong Kong-Macao Joint Laboratory for Environmental Pollution and Control, Guangzhou Institute of Geochemistry and Center for Excellence in Deep Earth Science, Chinese Academy of Science, Guangzhou 510640, China;

orcid.org/0000-0002-1982-0928

**Davide Vione** – Dipartimento di Chimica, Università degli Studi di Torino, 10125 Torino, Italy; orcid.org/0000-0002-2841-5721

Complete contact information is available at:  
<https://pubs.acs.org/10.1021/acs.est.1c01043>

## Notes

The authors declare no competing financial interest.

## ACKNOWLEDGMENTS

This study was financially supported by the National Natural Science Foundation of China (Nos. 41773131 and 41977187), Chinese Academy of Science, International Cooperation Grant (No. 132744KYSB20190007), State Key Laboratory of Organic Geochemistry, Guangzhou Institute of Geochemistry (SKLOG2020-5, and KTZ\_17101), and Guangdong Foundation for Program of Science and Technology Research (No. 2017B030314057).

## REFERENCES

- (1) Murphy, D. M.; Cziczo, D. J.; Froyd, K. D.; Hudson, P. K.; Matthew, B. M.; Middlebrook, A. M.; Peltier, R. E.; Sullivan, A.; Thomson, D. S.; Weber, R. J. Single-particle mass spectrometry of tropospheric aerosol particles. *J. Geophys. Res.: Atmos.* **2006**, *111*, No. D23S32.
- (2) Abbatt, J. P. D.; Lee, A. K. Y.; Thornton, J. A. Quantifying trace gas uptake to tropospheric aerosol: recent advances and remaining challenges. *Chem. Soc. Rev.* **2012**, *41*, 6555–6581.
- (3) Oros, D. R.; Simoneit, B. R. T. Identification and emission rates of molecular tracers in coal smoke particulate matter. *Fuel* **2000**, *79*, 515–536.
- (4) Schauer, J. J.; Rogge, W. F.; Hildemann, L. M.; Mazurek, M. A.; Cass, G. R.; Simoneit, B. R. T. Source apportionment of airborne particulate matter using organic compounds as tracers. *Atmos. Environ.* **1996**, *30*, 3837–3855.
- (5) Schauer, J. J.; Kleeman, M. J.; Cass, G. R.; Simoneit, B. R. T. Measurement of emissions from air pollution sources. 1. C1 through C29 organic compounds from meat charbroiling. *Environ. Sci. Technol.* **1999**, *33*, 1566–1577.
- (6) Schauer, J. J.; Kleeman, M. J.; Cass, G. R.; Simoneit, B. R. T. Measurement of emissions from air pollution sources. 4. C1–C27 organic compounds from cooking with seed oils. *Environ. Sci. Technol.* **2002**, *36*, 567–575.
- (7) Ren, L. J.; Fu, P. Q.; He, Y.; Hou, J. Z.; Chen, J.; Pavuluri, C. M.; Sun, Y. L.; Wang, Z. F. Molecular distributions and compound-specific stable carbon isotopic compositions of lipids in wintertime aerosols from Beijing. *Sci. Rep.* **2016**, *6*, No. 27481.
- (8) Tervahattu, H.; Juhanoja, J.; Vaida, V.; Tuck, A. F.; Niemi, J. V.; Kupiainen, K.; Kulmala, M.; Vehkamäki, H. Fatty acids on continental sulfate aerosol particles. *J. Geophys. Res. Atmos.* **2005**, *110*, No. D06207.
- (9) Feng, J.; Hu, M.; Chan, C. K.; Lau, P. S.; Fang, M.; He, L.; Tang, X. A Comparative Study of the Organic Matter in PM<sub>2.5</sub> from Three Chinese Megacities in three Different Climatic Zones. *Atmos. Environ.* **2006**, *40*, 3983–3994.
- (10) Dreyfus, M. A.; Johnston, M. V. Rapid Sampling of Individual Organic Aerosol Species in Ambient Air with the Photoionization Aerosol Mass Spectrometer. *Aerosol Sci. Technol.* **2008**, *42*, 18–27.
- (11) Zeng, J. F.; Yu, Z. J.; Mekic, M.; Liu, J.; Li, S.; Loisel, G.; Gao, W.; Gandolfo, A.; Zhou, Z.; Wang, X.; Herrmann, H.; Gligorovski, S.; Li, X. Evolution of indoor cooking emissions captured by using secondary electrospray ionization high resolution mass spectrometry. *Environ. Sci. Technol. Lett.* **2020**, *7*, 76–81.
- (12) Moise, T.; Rudich, Y. Reactive Uptake of Ozone by Aerosol-Associated Unsaturated Fatty Acids: Kinetics, Mechanism, and Products. *J. Phys. Chem. A* **2002**, *106*, 6469–6476.
- (13) Knopf, D. A.; Anthony, L. M.; Bertram, A. K. Reactive Uptake of O<sub>3</sub> by Multicomponent and Multiphase Mixtures Containing Oleic Acid. *J. Phys. Chem. A* **2005**, *109*, 5579–5589.
- (14) Hung, H.; Katrib, Y.; Martin, S. T. Products and Mechanisms of the Reaction of Oleic Acid with Ozone and Nitrate Radical. *J. Phys. Chem. A* **2005**, *109*, 4517–4530.
- (15) Robinson, A. L.; Subramanian, R.; Donahue, N. M.; Bernardo Bricker, A.; Rogge, W. F. Source Apportionment of Molecular Markers and Organic Aerosol. 3. Food Cooking Emissions. *Environ. Sci. Technol.* **2006**, *40*, 7820–7827.
- (16) McNeill, V. F.; Wolfe, G. M.; Thornton, J. A. The Oxidation of Oleate in Submicron Aqueous Salt Aerosols: Evidence of a Surface Process. *J. Phys. Chem. A* **2007**, *111*, 1073–1083.
- (17) Zahardis, J.; Petrucci, G. A. The oleic acid–ozone heterogeneous reaction system: products, kinetics, secondary chemistry, and atmospheric implications of a model system – a review. *Atmos. Chem. Phys.* **2007**, *7*, 1237–1274.
- (18) Vesna, O.; Sax, M.; Kalberer, M.; Gaschen, A.; Ammann, M. Product study of oleic acid ozonolysis as function of humidity. *Atmos. Environ.* **2009**, *43*, 3662–3669.
- (19) Sage, A. M.; Weitkamp, E. A.; Robinson, A. L.; Donahue, N. M. Reactivity of oleic acid in organic particles: changes in oxidant uptake and reaction stoichiometry with particle oxidation. *Phys. Chem. Chem. Phys.* **2009**, *11*, 7951–7962.
- (20) Chu, Y. X.; Chan, C. K. Reactive Uptake of Dimethylamine by Ammonium Sulfate and Ammonium Sulfate–Sucrose Mixed Particles. *Aerosol Sci. Technol.* **2017**, *51*, 988–997.
- (21) Nah, T.; Kessler, S. H.; Daumit, K. E.; Kröll, J. H.; Leoneabe, S. R.; Wilson, K. R. OH-initiated oxidation of sub-micron unsaturated fatty acid particles. *Phys. Chem. Chem. Phys.* **2013**, *15*, 18649–18663.
- (22) Schwartz-Narbonne, H.; Wang, C.; Zhou, S. M.; Abbatt, J. P. D.; Faust, J. Heterogeneous Chlorination of Squalene and Oleic Acid. *Environ. Sci. Technol.* **2019**, *53*, 1217–1224.
- (23) Baergen, A. M.; Donaldson, D. J. Photochemical renoxification of nitric acid on real urban grime. *Environ. Sci. Technol.* **2013**, *47*, 815–820.
- (24) Liu, J. P.; Li, S.; Mekic, M.; Jiang, H. Y.; Zhou, W. T.; Loisel, G.; Song, W.; Wang, X. M.; Gligorovski, S. Photoenhanced uptake of NO<sub>2</sub> and HONO formation on real urban grime. *Environ. Sci. Technol. Lett.* **2019**, *6*, 413–417.
- (25) Baergen, A. M.; Styler, S. A.; Van Pinxteren, D.; Müller, K.; Herrmann, H.; Donaldson, D. J. Chemistry of urban grime: Inorganic ion composition of grime vs. particles in Leipzig, Germany. *Environ. Sci. Technol.* **2015**, *49*, 12688–12696.
- (26) Chabas, A.; Lombardo, T.; Cachier, H.; Pertuisot, M. H.; Oikonomou, K.; Falcone, R.; Verità, M.; Geotti-Bianchini, F. Behaviour of self-cleaning glass in urban atmosphere. *Build. Environ.* **2008**, *43*, 2124–2131.
- (27) Zhou, X.; Gao, H.; He, Y.; Huang, G.; Bertman, S. B.; Civerolo, K.; Schwab, J. Nitric Acid Photolysis on Surfaces in Low NO<sub>x</sub> Environments: Significant Atmospheric Implications. *Geophys. Res. Lett.* **2003**, *30*, 2217.



- (28) Zhou, X.; Zhang, N.; TerAvest, M.; Tang, D.; Hou, J.; Bertman, S.; Alaghmand, M.; Shepson, P. B.; Carroll, M. A.; Griffith, S.; Dusanter, S.; Stevens, P. S. Nitric Acid Photolysis on Forest Canopy Surface as a Source for Tropospheric Nitrous Acid. *Nat. Geosci.* **2011**, *4*, 440–443.
- (29) George, C.; Strekowski, R. S.; Kleffmann, J.; Stemmler, K.; Ammann, M. Photoenhanced uptake of gaseous NO<sub>2</sub> on solid organic compounds: a photochemical source of HONO? *Faraday Discuss.* **2005**, *130*, 195–210.
- (30) Brigante, M.; Cazor, D.; D'Anna, B.; George, C.; Donaldson, D. J. Photoenhanced Uptake of NO<sub>2</sub> by Pyrene Solid Films. *J. Phys. Chem. A* **2008**, *112*, 9503–9508.
- (31) Ammar, R.; Monge, M. E.; George, C.; D'Anna, B. Photoenhanced NO<sub>2</sub> Loss on Simulated Urban Grime. *ChemPhysChem* **2010**, *11*, 3956–3961.
- (32) Sosedova, Y.; Rouvière, A.; Bartels-Rausch, T.; Ammann, M. UVA/Vis-induced nitrous acid formation on polyphenolic films exposed to gaseous NO<sub>2</sub>. *Photochem. Photobiol. Sci.* **2011**, *10*, 1680–1690.
- (33) Cazor, D.; Brigante, M.; Ammar, R.; D'Anna, B.; George, C. Heterogeneous Photochemistry of Gaseous NO<sub>2</sub> on Solid Fluoranthene Films: A Source of Gaseous Nitrous Acid (HONO) in the Urban Environment. *J. Photochem. Photobiol., A* **2014**, *273*, 23–28.
- (34) Stemmler, K.; Ammann, M.; Donders, C.; Kleffmann, J.; George, C. Photosensitized reduction of nitrogen dioxide on humic acid as a source of nitrous acid. *Nature* **2006**, *440*, 195–198.
- (35) Stemmler, K.; Ndour, M.; Elshorbany, Y.; Kleffmann, J.; D'Anna, B.; George, C.; Bohn, B.; Ammann, M. Light induced conversion of nitrogen dioxide into nitrous acid on submicron humic acid aerosol. *Atmos. Chem. Phys.* **2007**, *7*, 4237–4248.
- (36) Ndour, M.; D'Anna, B.; George, C.; Ka, O.; Balkanski, Y.; Kleffmann, J.; Stemmler, K.; Ammann, M. Photoenhanced uptake of NO<sub>2</sub> on mineral dust: Laboratory experiments and model simulations. *Geophys. Res. Lett.* **2008**, *35*, No. L05812.
- (37) Monge, M. E.; D'Anna, B.; George, C. Nitrogen dioxide removal and nitrous acid formation on titanium oxide surfaces—an air quality remediation process? *Phys. Chem. Chem. Phys.* **2010**, *12*, 8991–8998.
- (38) Monge, M. E.; D'Anna, B.; Mazri, L.; Giroir-Fendler, A.; Ammann, M.; Donaldson, D. J.; George, C. Light changes the atmospheric reactivity of soot. *Proc. Natl. Acad. Sci. U.S.A.* **2010**, *107*, 6605–6609.
- (39) Gómez Alvarez, E.; Soergel, M.; Gligorovski, S.; Bassil, S.; Bartolomei, V.; Coulomb, B.; Zetzsch, C.; Wortham, H. Light-induced nitrous acid (HONO) production from NO<sub>2</sub> heterogeneous reactions on household chemicals. *Atmos. Environ.* **2014**, *95*, 391–399.
- (40) Gandolfo, A.; Bartolomei, V.; Gómez Alvarez, E.; Tlili, S.; Gligorovski, S.; Kleffmann, J.; Wortham, H. The effectiveness of indoor photocatalytic paints on NO<sub>x</sub> and HONO levels. *Appl. Catal., B* **2015**, *84–90*.
- (41) Gandolfo, A.; Rouyer, L.; Wortham, H.; Gligorovski, S. The influence of wall temperature on NO<sub>2</sub> removal and HONO levels released by indoor photocatalytic paints. *Appl. Catal., B* **2017**, *209*, 429–436.
- (42) Liu, J.; Deng, H.; Lakey, P. S. J.; Jiang, H.; Mekic, M.; Wang, X.; Shiraiwa, M.; Gligorovski, S. Unexpectedly High Indoor HONO Concentrations Associated with Photochemical NO<sub>2</sub> Transformation on Glass Windows. *Environ. Sci. Technol.* **2020**, *54*, 15680–15688.
- (43) Liu, J.; Deng, H.; Sheng, L.; Jiang, H.; Mekic, M.; Zhou, W.; Wang, Y.; Loisel, G.; Wang, X.; Gligorovski, S. Light-Enhanced Heterogeneous Conversion of NO<sub>2</sub> to HONO on Solid Films Consisting of Fluorene and Fluorene/Na<sub>2</sub>SO<sub>4</sub>: An Impact on Urban and Indoor Atmosphere. *Environ. Sci. Technol.* **2020**, *54*, 11079–11086.
- (44) Han, C.; Yang, W.; Wu, Q.; Yang, H.; Xue, X. Heterogeneous photochemical conversion of NO<sub>2</sub> to HONO on the humic acid surface under simulated sunlight. *Environ. Sci. Technol.* **2016**, *50*, 5017–5023.
- (45) Zhou, S.; Young, C. J.; VandenBoer, T. C.; Kowal, S. F.; Kahan, T. F. Time-resolved measurements of nitric oxide, nitrogen dioxide, and nitrous acid in an occupied New York home. *Environ. Sci. Technol.* **2018**, *52*, 8355–8364.
- (46) Brigante, M.; Cazor, D.; D'Anna, B.; George, C.; Donaldson, D. J. Photoenhanced Uptake of NO<sub>2</sub> by Pyrene Solid Films. *J. Phys. Chem. A* **2008**, *112*, 9503–9508.
- (47) Yu, Z.; Liu, C.; Niu, H.; Wu, M.; Gao, W.; Zhou, Z.; Huang, Z.; Li, X. Real time analysis of trace volatile organic compounds in ambient air: a comparison between membrane inlet single photon ionization mass spectrometry and proton transfer reaction mass spectrometry. *Anal. Methods* **2020**, *12*, 4343–4350.
- (48) Liu, J.; Li, S.; Zeng, J.; Mekic, M.; Yu, Z.; Zhou, W.; Loisel, G.; Gandolfo, A.; Song, W.; Wang, X.; Zhou, Z.; Herrmann, H.; Li, X.; Gligorovski, S. Assessing indoor gas phase oxidation capacity through real-time measurements of HONO and NO<sub>x</sub> in Guangzhou, China. *Environ. Sci.: Processes Impacts* **2019**, *21*, 1393–1402.
- (49) Mekic, M.; Zeng, J.; Jiang, B.; Li, X.; Lazarou, Y. G.; Brigante, M.; Herrmann, H.; Gligorovski, S. Formation of toxic unsaturated multifunctional and organosulfur compounds from the photo-sensitized processing of fluorene and DMSO at the air-water interface. *J. Geophys. Res.: Atmos.* **2020**, *125*, No. e2019JD031839.
- (50) Atkinson, R. Atmospheric chemistry of VOCs and NO<sub>x</sub>. *Atmos. Environ.* **2000**, *34*, 2063–2101.
- (51) Atkinson, R.; Arey, J. Atmospheric Degradation of Volatile Organic Compounds. *Chem. Rev.* **2003**, *103*, 4605–4638.
- (52) Tang, I. N.; Munkelwitz, H. R. Water activities, densities, and refractive indices of aqueous sulfates and sodium nitrate droplets of atmospheric importance. *J. Geophys. Res.: Atmos.* **1994**, *99*, 18801–18808.
- (53) Mekic, M.; Wang, Y.; Loisel, G.; Vione, D.; Gligorovski, S. Ionic Strength Effect Alters the Heterogeneous Ozone Oxidation of Methoxyphenols in Going from Cloud Droplets to Aerosol Deliquescent Particles. *Environ. Sci. Technol.* **2020**, *54*, 12898–12907.
- (54) Mekic, M.; Loisel, G.; Zhou, W.; Jiang, B.; Vione, D.; Gligorovski, S. Ionic-Strength Effects on the Reactive Uptake of Ozone on Aqueous Pyruvic Acid: Implications for Air–Sea Ozone Deposition. *Environ. Sci. Technol.* **2018**, *52*, 12306–12315.
- (55) *American Society for Testing and Materials G-173-03 Reference Spectra*; National Renewable Energy Laboratory (NREL), 2003.
- (56) Gandolfo, A.; Gligorovski, V.; Bartolomei, V.; Gomez Alvarez, E.; Tlili, S.; Wortham, H.; Kleffmann, J.; Gligorovski, S. Spectrally resolved actinic flux and photolysis frequency of key species within indoor environment. *Build. Environ.* **2016**, *109*, 50–57.
- (57) Brauer, M.; Dumyahn, T. S.; Spengler, J. D.; Gutschmidt, K.; Heinrich, J.; Wichmann, H. E. Measurement of acidic aerosol species in eastern Europe: implications for air pollution epidemiology. *Environ. Health Perspect.* **1995**, *103*, 482–488.
- (58) Rasmussen, T. R.; Brauer, M.; Kjaergaard, S. Effects of nitrous acid exposure on human mucous membranes. *Am. J. Respir. Crit. Care Med.* **1995**, *151*, 1504–1511.
- (59) Gómez Alvarez, E.; Amedro, D.; Afif, S.; Gligorovski, S.; Schoemacker, C.; Fittschen, C.; Doussin, J. F.; Wortham, H. Unexpectedly high indoor hydroxyl radical concentrations associated with nitrous acid. *Proc. Natl. Acad. Sci. U.S.A.* **2013**, *110*, 13294–13299.
- (60) Lee, J. D.; Whalley, L. K.; Heard, D. E.; Stone, D.; Dunmore, R. E.; Hamilton, J. F.; Young, D. E.; Allan, J. D.; Laufs, S.; Kleffmann, J. Detailed budget analysis of HONO in central London reveals a missing daytime source. *Atmos. Chem. Phys.* **2016**, *16*, 2747–2764.
- (61) Shi, X. W.; Ge, Y. F.; Zheng, J.; Ma, Y.; Ren, X. R.; Zhang, Y. C. Budget of nitrous acid and its impacts on atmospheric oxidative capacity at an urban site in the central Yangtze River Delta region of China. *Atmos. Environ.* **2020**, *238*, No. 117725.
- (62) Liu, J. Y.; Liu, Z. R.; Ma, Z. Q.; Yang, S. H.; Yao, D.; Zhao, S. M.; Hu, B.; Tang, G. Q.; Sun, J.; Cheng, M. T.; Xu, Z. J.; Wang, Y. S. Detailed budget analysis of HONO in Beijing, China: Implication on atmosphere oxidation capacity in polluted megacity. *Atmos. Environ.* **2020**, *244*, No. 117957.

(63) Nissenson, P.; Dabdub, D.; Das, R.; Maurino, V.; Minero, C.; Vione, D. Evidence of the water-cage effect on the photolysis of  $\text{NO}_3^-$  and  $\text{FeOH}^{2+}$ . Implications of this effect and of  $\text{H}_2\text{O}_2$  surface accumulation on photochemistry at the air-water interface of atmospheric droplets. *Atmos. Environ.* **2010**, *44*, 4859–4866.

(64) Zhang, X.; Barraza, K. M.; Upton, K. T.; Beauchamp, J. L. Time resolved study of hydroxyl radical oxidation of oleic acid at the air-water interface. *Chem. Phys. Lett.* **2017**, *683*, 76–82.

(65) Freeman, B. A.; Baker, P. R. S.; Schopfer, F. J.; Woodcock, S. R.; Napolitano, A.; d'Ischia, M. Nitro-fatty Acid Formation and Signaling. *J. Biol. Chem.* **2008**, *283*, 15515–15519.

(66) Jain, K.; Sidda, A.; Marathi, A.; Roy, U.; Falck, J. R.; Balazy, M. The mechanism of oleic acid nitration by  $\text{NO}_2$ . *Free Radic. Biol. Med.* **2008**, *45*, 269–283.

(67) Huie, R. E. The reaction kinetics of  $\text{NO}_2$ . *Toxicology* **1994**, *89*, 193–216.

(68) Pryor, W. A.; Lightsey, J. W.; Church, D. F. Reaction of Nitrogen Dioxide with Alkenes and Polyunsaturated Fatty Acids: Addition and Hydrogen Abstraction Mechanisms. *J. Am. Chem. Soc.* **1982**, *104*, 6685–6692.

(69) Bedini, A.; Maurino, V.; Minero, C.; Vione, D. Theoretical and experimental evidence of the photonitration pathway of phenol and 4-chlorophenol: A mechanistic study of environmental significance. *Photochem. Photobiol. Sci.* **2012**, *11*, 418–424.

(70) Minero, C.; Maurino, V.; Bono, F.; Pelizzetti, E.; Marinoni, A.; Mailhot, G.; Carlotti, M. E.; Vione, D. Effect of selected organic and inorganic snow and cloud components on the photochemical generation of nitrite by nitrate irradiation. *Chemosphere* **2007**, *68*, 2111–2117.

(71) Guan, C.; Li, X.; Zhang, W.; Huang, Z. Identification of Nitration Products during Heterogeneous Reaction of  $\text{NO}_2$  on Soot in the Dark and under Simulated Sunlight. *J. Phys. Chem. A* **2017**, *121*, 482–492.

(72) Bejan, I.; Abd El Aal, Y.; Barnes, I.; Benter, T.; Bohn, B.; Wiesen, P.; Kleffmann, J. The photolysis of ortho-nitrophenols: a new gas phase source of HONO. *Phys. Chem. Chem. Phys.* **2006**, *8*, 2028–2035.

(73) Lee, J. D.; Whalley, L. K.; Heard, D. E.; Stone, D.; Dunmore, R. E.; Hamilton, J. F.; Young, D. E.; Allan, J. D.; Laufs, S.; Kleffmann, J. Detailed budget analysis of HONO in central London reveals a missing daytime source. *Atmos. Chem. Phys.* **2016**, *16*, 2747–2764.

(74) Sumlin, B. J.; Pandey, A.; Walker, M. J.; Pattison, R. S.; Williams, B. J.; Chakrabarty, R. K. Atmospheric Photooxidation Diminishes Light Absorption by Primary Brown Carbon Aerosol from Biomass Burning. *Environ. Sci. Technol. Lett.* **2017**, *4*, 540–545.